1 BIOINSPIRED HELICOIDAL COMPOSITE STRUCTURE 2 FEATURING FUNCTIONALLY GRADED VARIABLE PLY PITCH

3 F.Rizzo, M.Portus, F.Pinto, M. Meo

Material and Structure Centre, Department of Mechanical Engineering,

University of Bath, Bath, UK

Abstract

4

5

6

7

8

9

10

11

12

13

14

15

16

17

18

19

20

21

22

23

24

25

26

27

28

29

30

Composite laminated materials have been largely implemented in advanced applications due to the high tailorability of their mechanical performance and low weight. However, due to their low resistance against out of plane loading they are prone to generate damage as consequence of an impact event, leading to the loss of mechanical properties and eventually to the catastrophic failure of the entire structure. In order to overcome this issue, the high tailorability can be exploited to replicate complex biological structures that are naturally optimised to withstand extreme impact loading. Bioinspired helicoidal laminates have been already studied in-depth with good results, however they have been manufactured by applying a constant pitch rotation between each consecutive ply. This is in contrast with what observed in biological structures where this pitch rotation is not constant along the thickness, but it gradually increases from the outer shell to the inner core in order to optimise energy absorption and stress distribution. Based on this concept, Functionally Graded Pitch (FGP) laminated composites were designed and manufactured in order to improve the impact resistance relative to a benchmark laminate exploiting the tough nature of helicoidal structures with variable rotation angles. To the authors' knowledge, this is one of the first attempts to fully reproduce the helicoidal arrangement found in nature using a mathematically scaled form of the triangular sequence to define the lamination layup. Samples were subject to three-point bending and tested under Low Velocity Impact (LVI) conditions at 15J and 25J impact energies and ultrasonic testing was used to evaluate the damaged area. Flexural After Impact (FAI) tests were used to evaluate the post-impact residual energy to confirm the superior impact resistance offered by these bioinspired structures. Vast improvements in impact behaviour were observed in FGP laminates over the benchmark, with an average reduction of 41% of the damaged area and an increase of post-impact residual energy of 111%. Absorbed energy was similarly reduced (-44%), and greater mechanical strength (+21%) and elastic energy capacity (+78%) were demonstrated in three-point bending testing.

Keywords: impact resistance, residual strength, bioinspiration, helicoidal, composite

1 Literature Review

31

32

33

34

35

36

37

38

39

40

41

42

43

44

45

46

47

48

49

50

51

52

53

54

55

56

57

58

59

60

61

62

63

Laminated composite materials are used in engineering to take advantage of the high specific strength and stiffness they can provide, in addition to their excellent fatigue and corrosion resistance. A notable disadvantage in many laminated composites, however, is their susceptibility towards out of plane loading with the generation of damage within the structure such as delamination, crack and fibre failure. This can greatly affect the performance of the part and could lead to the sudden and catastrophic collapse of the entire system [1]. In order to overcome this issue, several solutions can be found in literature aiming to increase the impact properties of these materials, including single components modification [2-4], hybridisation with metal wires [5], the introduction of non-newtonian fluids [6] and the use of polymeric coating as superficial protective layer [7]. In this context, biological structures such nacre [8], the cuticle of the Scarabaei Beetle [9] and the dactyl club of the Mantis Shrimp [10] constitute a very interesting source of inspiration since they naturally evolved to function as impact-resistant armour and weaponry for protection and hunting. For instance, nacre structure shows a brick-and-mortar inner configuration in which strain-hardening features are activated during failure [11, 12] while beetle cuticle are organised in a constant pitch helicoidal structure formed by a constant rotation of the layers through the thickness – also known as a "Bouligand" structure [13-15]. Extensive research has been focused on the investigation of the behaviour of the helicoidal structure under dynamic conditions showing improved impact resistance as result of the activation of an additional energy dissipation mechanism called crack twisting [9]. This mechanism promotes the formation of microcracks which follow the helicoidal orientation of the layers creating a twisted crack front dissipating a higher amount of energy in a longer crack path without severe detriment of the mechanical properties and/or catastrophic failure [16]. The effectiveness in mimicking the crack twisting mechanisms in composites were investigated by Suksangpanya et al. [17], who used 3D printing to create a structure representing a helicoidally laminated composite. Three-point bending tests were then carried out on the structures to investigate damage mechanisms, resulting in twisting cracks through the matrix with no fracture of fibres. This research highlights the changing damage mechanisms through the thickness of composites, which is also dependent on the constituent fibre and matrix properties in addition to the stacking sequence of the laminate. Shang et al. [18] conducted flexural testing on circular helicoidal laminate plates finding improved mechanical performance using small angle in the helicoidal structures in comparison with cross ply laminates. Ginzburg et al. [19] instead experimentally and numerically evaluated the impact performance of helicoidal laminates using different stacking-up sequence featuring small pitch angle. The authors observed a reduced damaged area at similar values of absorbed energy reporting a higher damage tolerance when helicoidal laminates were compared to cross-ply and quasi-isotropic ones. This confirms that the activation of the crack twisting mechanism also for this study case reporting a less detrimental effect of the damage on the residual mechanical properties of the bioinspired laminates in comparison with traditional ones.

However, even though excellent results have been obtained, these biological structures (i.e. Dactyl club structure of Shrimp Mantis) can still offer a precious source of inspiration for bioinspired composites and a further significant step-forward in the development of impact-resistant laminates.

71

72

73

74

75

76

77

78

79

80

81

82

83

84

85

86

87

88

89

90

91

92

93

94

95

96

Indeed, research widely investigated only a partial aspect of the Shrimp Mantis complex structure i.e. the simple helicoidal layup in designing bioinspired materials while only little research has, instead, been completed into the full-inspiration and replication of this biological structure to exploit its full potential in preventing impact damage. Indeed, Mantis structure composes of a complex macrogeometry which includes periodic and striated regions: whilst striated regions - composed of aligned mineral fibres arranged in a circumferential band to avoid lateral expansion of the structure during strike - aid the structural stability of the dactyl club, previous research has concluded the periodic region – composed of protein fibres in laminated periodic pattern - is fundamental in the energy dissipation and impact resistance [20]. Moreover, scanning electron microscopy on the dactyl club has indeed revealed an interesting variation of inter-ply pitch angles in the periodic region. In particular, the biological structure increases in pitch from 1.6° closest to the impact region to 6.2° at the innermost region of the club in a near-linear manner [9, 20]. This small angle variation not only is able to activate the aforementioned crack twisting mechanism seen in the Scarabaei cuticle, but also changes the mechanical properties of the laminate along its thickness creating a Functionally Graded (FG) material [21] showing unique behaviour in terms of dynamic response [22] and failure mechanisms [23] including crack propagation [24] and delamination [25]. Bamboo [26], human bones [27], alligator osteoderm [28] are only few examples of the numerous FG structures that can be found in nature. These biological structures evolved their configuration towards the satisfaction of specific structural requirements in order to ensure the survival of the entire biological system by tuning heterogeneous structural parameters across material's thickness such as composition [29, 30], arrangement [28, 31] dimension [32, 33] and orientation [34, 35]. This affects the mechanical properties in specific regions of the structure allowing to optimise the response in function of a determined solicitation (predator's attack, environmental threat, ...). Another important characteristic typical of FG materials is the presence of a gradual and smooth variation of the properties in the areas comprised between the functionalised regions in order to reduce stress localisation in correspondence of their interfaces and maximise the overall performance of the system.

Focusing the attention on FG materials featuring a functional variation of its components' orientation, the body armour of Arapaima gigas fish can be considered as one of the possible examples. This structure is composed by lamellae which cartilaginous fibrils are tilted by ~35° from the adjacent ones. This maximises the impact and penetration resistance of the system against foreign objects by the activation of crack twisting mechanisms similar to the ones previously described for Bouligand structures. Consequently, as confirmed by [26], it is evident that a connection between FG material with functional orientation and Bouligand structures can be found considering this latter as a subcategory of FG materials.

Several researchers focused their attention in replicating the unique impact resistance and failure mechanisms of FG biological structures featuring functional orientation in laminated composites.

This work is focused on the design and development of a bioinspired helicoidal composite characterised by a graded pitch angle which exhibits improved impact behaviour whilst maintaining high mechanical properties. Utilising this variable angle ply replicated from the inner structure of dactyl club of Shrimp Mantis, smaller angles of rotation were located in proximity of the laminate surface in order to improve damage tolerance via the activation of enhanced crack twisting mechanisms during an impact event. The mechanical strength, stiffness, and impact properties of laminates were evaluated by experimental testing to assess and prove the potential of these bioinspired Functionally Graded Pitch (FGP) helicoidal structures in advanced applications while ultrasound techniques were used to evaluate the damaged areas and correlate their extent with the residual mechanical properties evaluated using experimental post-impact testing.

2 Functionally Graded Pitch (FGP) laminates

In order to mimic the unique structure of the Shrimp Mantis and obtain a high-performance bioinspired laminated composite, a deep understanding of the enhanced failure mechanisms of helicoidal laminates is fundamental to design the stacking sequence of these materials and maximise their potentialities towards impact events. In this section, firstly a systematic analysis of the aforementioned crack twisting mechanism will be illustrated (Section 2.1). Afterwards, the design used in this work will be presented (section 2.2) with focus on the issues found during the replication of biological structure into the laminated one. In Section 2.3, the analysis of these limitations and the adequate solution is presented.

2.1 Mechanical performance

In laminated composites, three main damage typologies can be identified as main cause of failure: fibre failure, intralaminar fracture (matrix cracking) and interlaminar fracture (delamination). Crack-twisting is a failure mechanism generated by the presence of small ply angle between two different layers of the material based on the principle that cracks tend to propagate along the path that requires the lowest amount of energy to generate new surfaces [36]. It can be explained focusing the attention on the delamination fracture energy and its dependency from the ply orientation. Indeed, even though the critical energy for intralaminar fracture can be considered almost constant in function of the ply angle, the critical energy for the interlaminar one strongly depends on the ply angle between two adjacent layers as reported by several authors [37-39]. This concept is experimentally investigated by Kim [40] who reported that the interlaminar fracture toughness can be associated with the mixed mode fracture toughness G expressed as:

$$G = G_I + G_{II} \tag{1}$$

where G_I and G_{II} are the Mode I and Mode II fracture toughness (kJ/m²) experimentally evaluated using Mixed Mode Bending (MMB) tests. The values of these two toughness can be then calculated from the experimental data using equations (2) and (3) [40]:

$$G_I = \frac{(F(3s-l))^2}{16bl^2 E_{11f}I} (a+h)^2$$
 (2)

$$G_{II} = \frac{3(F(c+l))^2}{64bl^2 E_{11f}I} (a+0.42h)^2$$
(3)

where F is the maximum force recorded before the load drop, a and s are the initial delamination and span lengths respectively; 1, h and b are half of the length, thickness and width of the sample respectively. E_{11f} is the flexural elastic modulus in the direction of the fibres while I is the area moment of inertia of one of the delaminated portions. Several stacking up configuration at different ply angles were tested in this work reporting accurate results regarding the dependency of G on the difference in angle orientation between two adjacent plies. Afterwards, the relationship between G_I and G_{II} and the delamination fracture toughness G_c can be obtained by using the following semi empirical formulation:

$$G_c = A + BG_H G^m (4)$$

where A, B and m are the coefficients extrapolated via the non-linear regression (power law) of the experimental data. Thus, following this approach, it is possible to experimentally correlate the ply orientation used in the stacking-up of the laminate to the G_c value. Results clearly showed that that delamination fracture toughness is inversely proportional to the angle ply. In particular, the authors showed that two adjacent plies with a mismatch angle of 90° have a reduction of ~50% in terms of fracture toughness in comparison with a mismatch angle of 0° . Another result reported in this work is that the G_c dependency on the ply angle is also strongly influenced by loading conditions applied to the laminate: the closer to the pure Mode II loading, the stronger the dependency of G_c on the ply orientation. Following the same concept, Anderson et al. [38] also investigated the relationship between G_c and ply orientation and proposed an equation to approximate the G_{IIc} value from the ply angle θ and the value of fracture toughness with $\theta = 0^\circ$ (G_{II0}). They concluded that it is possible to predict the Mode II interlaminar fracture toughness by using the formula:

$$G_{IIc} = G_{II0} + Btan\theta \tag{5}$$

where B is a coefficient that takes into account the additional shear stress contribution. Considering the loading conditions found in impact events, the main cause of failure within the composite structure can be related to the shear stress [41-43] localised within a structure during the dynamic loading. Consequently, it is possible to assume that Mode II failure is dominant and high dependency from the ply angle is expected for the G_c value in this loading condition.

Following these considerations and analysing the effect of ply angle on the failure behaviour of composite materials, it is possible to observe that the smaller the angle used between two consecutive plies, the higher the delamination fracture toughness. On the other hand, increasing the ply angle, the delamination fracture toughness decreases. Hence, when the angle between two adjacent plies changes by a large quantity, the crack prefers to propagate along the interlayer interface instead of generating intralaminar cracks since the fracture energy required for creating delamination is lower. On the other hand, when smaller angles are used, the energy required to propagate the damage along the interface is higher and consequently, it is energy-wise easier for the crack to propagate across the matrix of the layer following the ply angle and "jump" across the interface between layers [10]. A schematisation of this concept is reported in Figure 1 where an helicoidal laminate is compared to a traditional one showing their differences in terms of failure mechanisms.

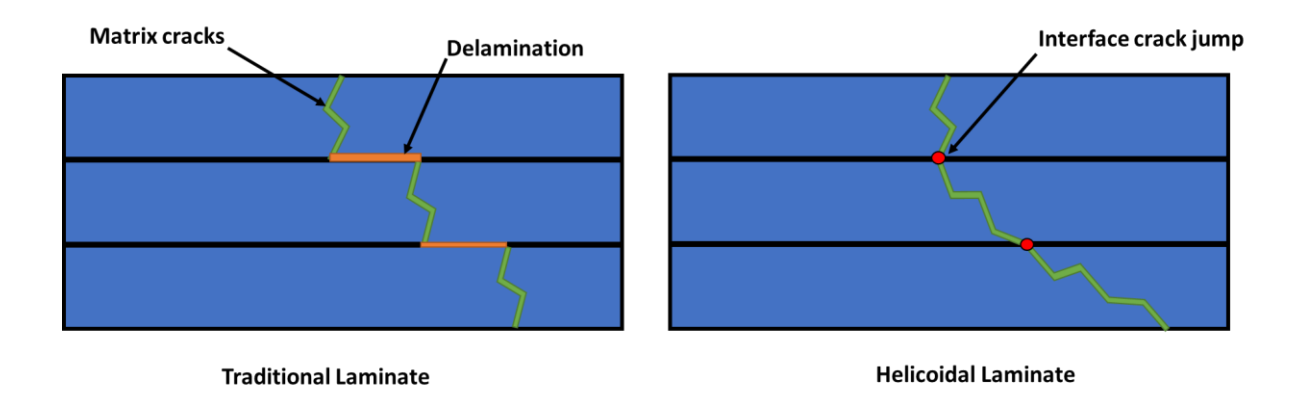


Figure 1- Illustration of the crack twisting mechanisms for helicoidal laminates' failure

This was confirmed by Liu et al. [44] in their experimental study on helicoidal laminates, in which they report that larger delaminated areas are generated within laminates with large ply angle since the interlaminar shear strength lowers its value accordingly with the increase of angle. Consequently, the use of helicoidal configurations with small ply angle reduces the extent and number of delaminated areas if compared with traditional ones allowing the system to tolerate higher contact force while dissipating a similar amount of impact energy [19, 45]. Another aspect of this behaviour is also the generation of subcritical damaged areas [16] within the laminate, a typology of damage that shows reduced effects on the performance of the laminate with no sign of critical failure and load drops. This enables the structure to absorb a higher amount of energy and tolerate higher contact force than traditional laminates.

While it is clear that the helicoidal configuration improves out of plane properties, it is important to notice that a decrease of out-of-plane stiffness is observed when a small ply angle is used due to the reduced number of plies oriented along the principal directions of the laminate [46]. In particular, by increasing the ply angle, it is possible to increase the stiffness of the material, but the effectiveness of the crack twisting mechanisms is reduced. A compromise between in-plane (stiffness) and out of plane (crack twisting) is then necessary.

This compromise is found in the use of FGP angle across the thickness's direction of the laminate as seen in FG materials. Indeed, using a small ply angle in the proximity of the impact event, it is possible to promote crack twisting mechanisms and, thus, enhance the damage tolerance of laminate via the creation of sub-critical damage. When an impact happens, crack and delamination opening initiates and firstly propagates in these regions maximising the effect of the crack twisting mechanisms and dissipating most of the energy received from the impact event. Increasing the distance from the impact event, since most of the impact energy has been already absorbed in the upper portion of the laminate

and, consequently, no significant delaminated areas can be generated in this portion, the increased pitch angle has the function to limit the in plane stiffness reduction.

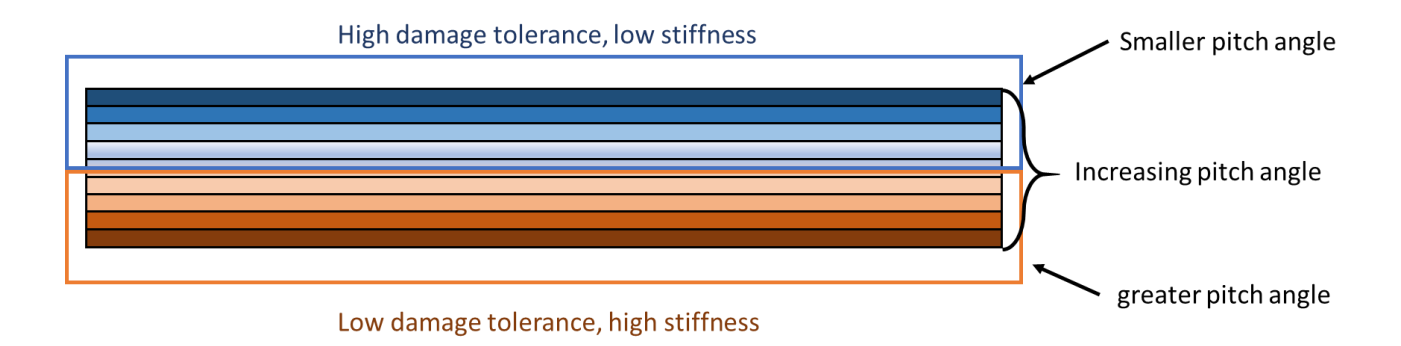


Figure 2- Schematisation of the mechanical behaviour of FGP laminates

Based on these considerations, the use of FGP represents a cutting-edge solution for the creation of high-performance bioinspired composites to satisfy requirements of advanced application in which high load and damage tolerances are fundamental for the safety and reliability of the primary load-bearing structures.

2.2 Design description

Due to the nature of the thin laminae in biological composites and the gradual development of these complex biological structures across the growing process of the organism, it is not practically possible to manufacture a fully accurate biomimetic composite from synthetic CFRP material. This is due to the intrinsic nature of composites manufacturing that requires the use of temperature and pressure that can create distortion or geometrical defect if not carefully carried out. Consequently, to enable the manufacturing of helicoidal composite structures with a reasonable thickness and closely mimic the dactyl club structure of Mantis Shrimp, the pitch angle change of the composite was completed over one full rotation of constituent laminae – a notable difference to the biological structure which completes this change over many complete rotations [47]. The ply angle was increased along the laminate's thickness following a mathematically scaled triangular sequence as observed in literature [48]. The formula used to define the sequence is reported in equation 6.

$$c\sum_{k=1}^{n} 1 + 2 + 3 + 5 + \dots = c\frac{n(n+1)}{2}$$
(6)

where c is the scaling coefficient.

Based on this formula, the Functionally Graded Asymmetric (FGPA) lamination sequence (Figure 3.a) was designed with an initial small ply angle (~1.2-1.8°). However, due to the asymmetrical layup sequence used during the manufacturing process, the presence of thermal warpage (Appendix A) can represent a technical and geometrical issue for this structure.

Thus, a Functionally Graded Pitch Symmetric (FGPS) lamination sequence (Figure 3.b) was also investigated to examine if the mechanisms can be implemented without warpage utilising the same number of layers as in the asymmetrical layup.

The lamination sequences for FGPA and FGPS configurations considered for this work are reported in Table 1.

Table 1-Bio-inspired Composite Designs Based on Mantis Shrimp Dactyl Club

Lay-up Title	Ply Structure
Benchmark	[0/0/+45/-45/90/0/+45/-45/90]s
FGPS (c=1.2)	[0/5/15/30/50/75/105/140/180] _s
FGPA (c=5)	[0/1.2/3.5/7.1/11.8/17.7/24.7/32.9/42.4/52.9/64.7/77.6/91.8/107.1/123.5/141.2/160/180]

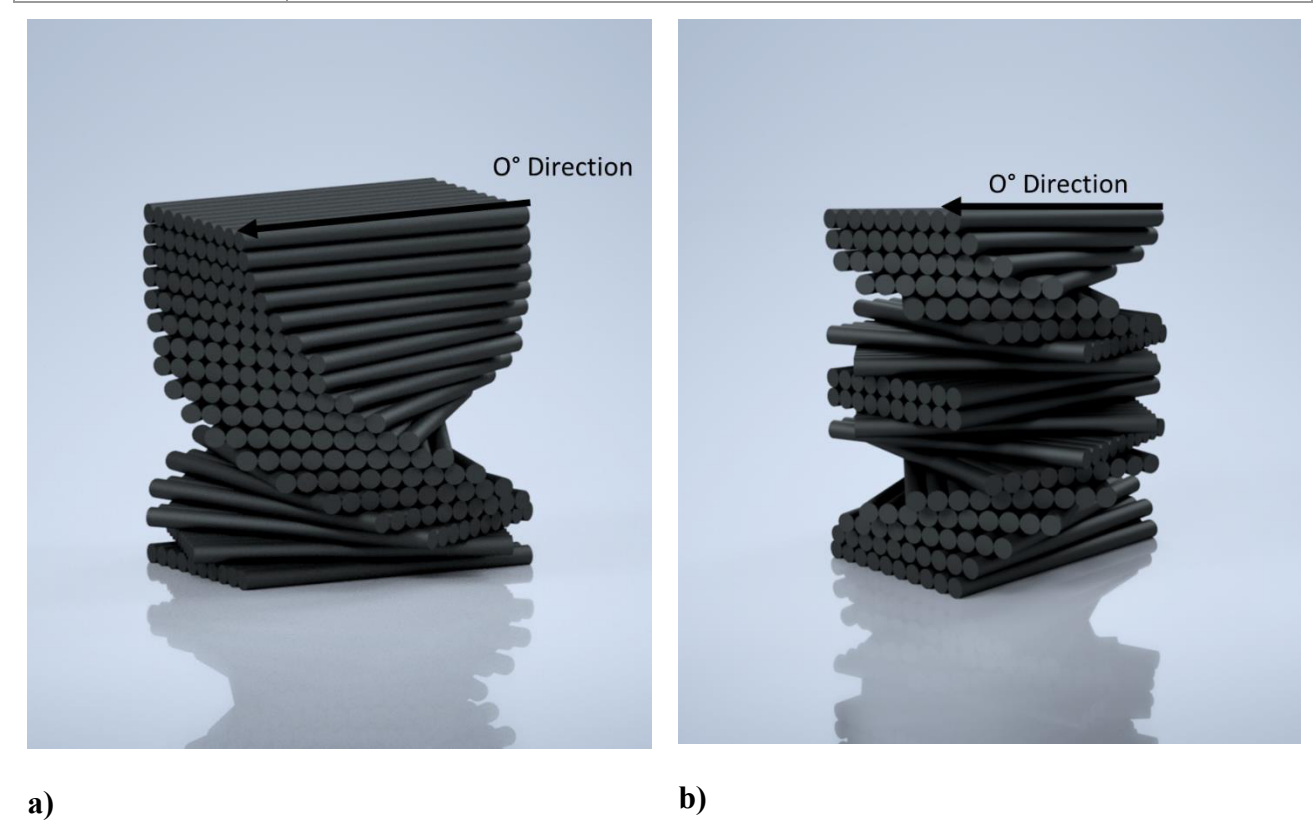


Figure 3-Layout of the designed helicoidal structures: a) Asymmetric (FGPA) and b) Symmetric (FGPS)

3 Materials and Methods

3.1 Sample Manufacturing

For the experimental analysis of the FGP design, unidirectional carbon fibre prepreg "XPREG® XC130" was used. Each ply was cut into 100mm x 150mm for the impact test and 90mm x 270mm for the bending samples. The lamination sequences used for the different configurations are reported in Table 1 and the all the laminates were cured using the temperature cycle shown in Figure 4 in order to minimise the residual stresses [49] generated by the FGPA design (Appendix A). The final thickness of the samples is ~5.2 mm using 18 plies in total.

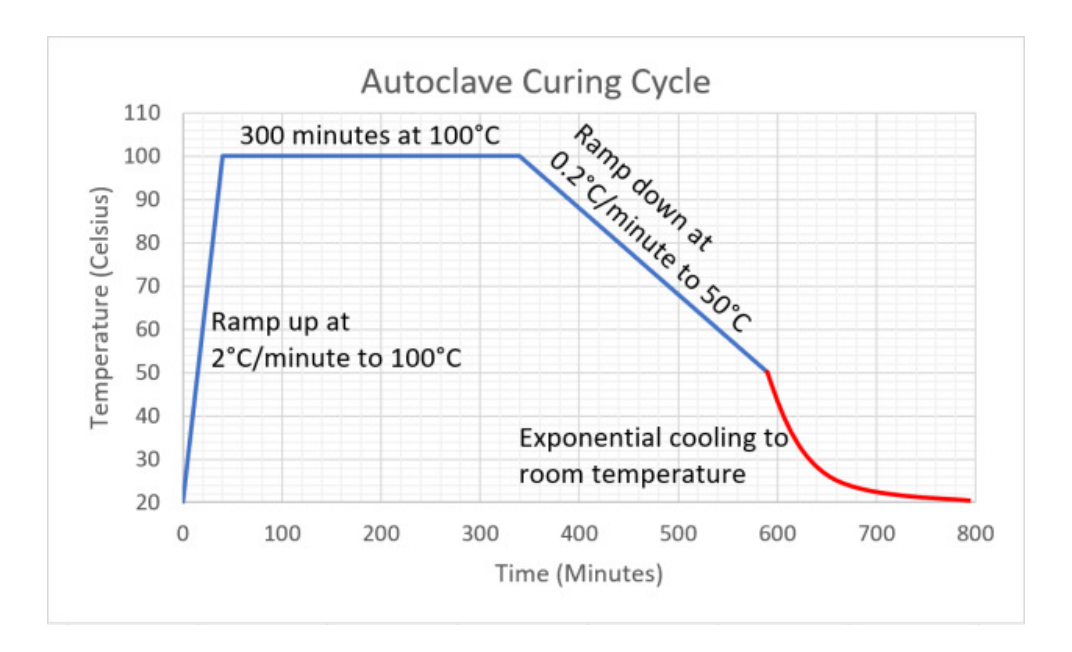
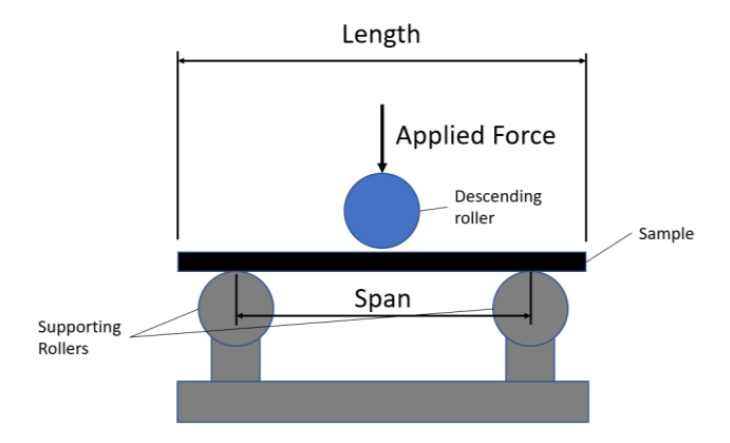


Figure 4- Autoclave Cooling Cycle

3.2 Three points bending

Flexural properties of the different laminates were determined by three-point bending (Figure 5), following the ISO 14125:1998+A1 guidelines and using a universal Instron testing machine model 3369 with a 50kN load cell. Due to the quasi-static nature of impacts with high ratio of impactor mass to equivalent structure mass [50], the static flexure test aids understanding of the different damage mechanisms involved during the material failure.



251 Figure 5- Three Point Bending Illustration

252

253

254

262

263

264

Supports and loading rollers of radius 5 ± 0.2 mm were used with a loading speed of 13.76 mm/min, in accordance with Equation (18) for a strain rate of 0.01 mm/min and 5.16 mm average sample thickness.

$$v = \frac{\varepsilon' L^2}{6h} \tag{18}$$

In these equation v is loading speed (mm/min), ε ' is strain rate, L is span length (mm), h is laminate thickness (mm). With a span of 206.5mm and a 50kN load cell used, fixed rate three-point bending tests were completed with time, load, and deflection data logged. Flexural stress and strain data were calculated with equations (19)-(20) considering individual sample width and thicknesses.

$$\sigma_f = \frac{3FL}{2bh^2} \tag{19}$$

$$\varepsilon_f = \frac{6sh}{L^2} \tag{20}$$

where: σ_f is flexural stress [MPa], F is applied load [N], b is laminate width [mm], ε_f is flexural strain and s is central displacement [mm]. Considering the load data at flexural strains of 0.0005 and 0.0025, the flexural modulus was calculated using the equation (21):

$$E_f = \frac{L^3}{4bh^3} \left(\frac{\Delta F}{\Delta s}\right) \tag{21}$$

where E_f is flexural modulus (GPa), ΔF is difference in force between strains, Δs is difference in central displacement between strains. The Specific Elastic Energy (SEE) done normalised by the stressed volume of sample was calculated per equation (22)

$$w_i = \frac{\int_0^{x_i} F \, dx}{dhL} \tag{22}$$

where wi is instantaneous cumulative specific work done (J), x is midpoint compression, x_i is instantaneous midpoint compression and F is midpoint load.

3.3 Low Velocity Impact

Impact tests were carried out on 100x150mm impact samples with a drop rig of adjustable impactor mass and drop height as shown in Figure 6. An oscilloscope (PICO TECHNOLOGY Picoscope) and a MATLAB code were used to collect and process the impact signal from a KISTLER loadcell. A 15mm diameter semi-spherical hardened steel impactor tip was used according to the ISO 6603-2:2000 standard.

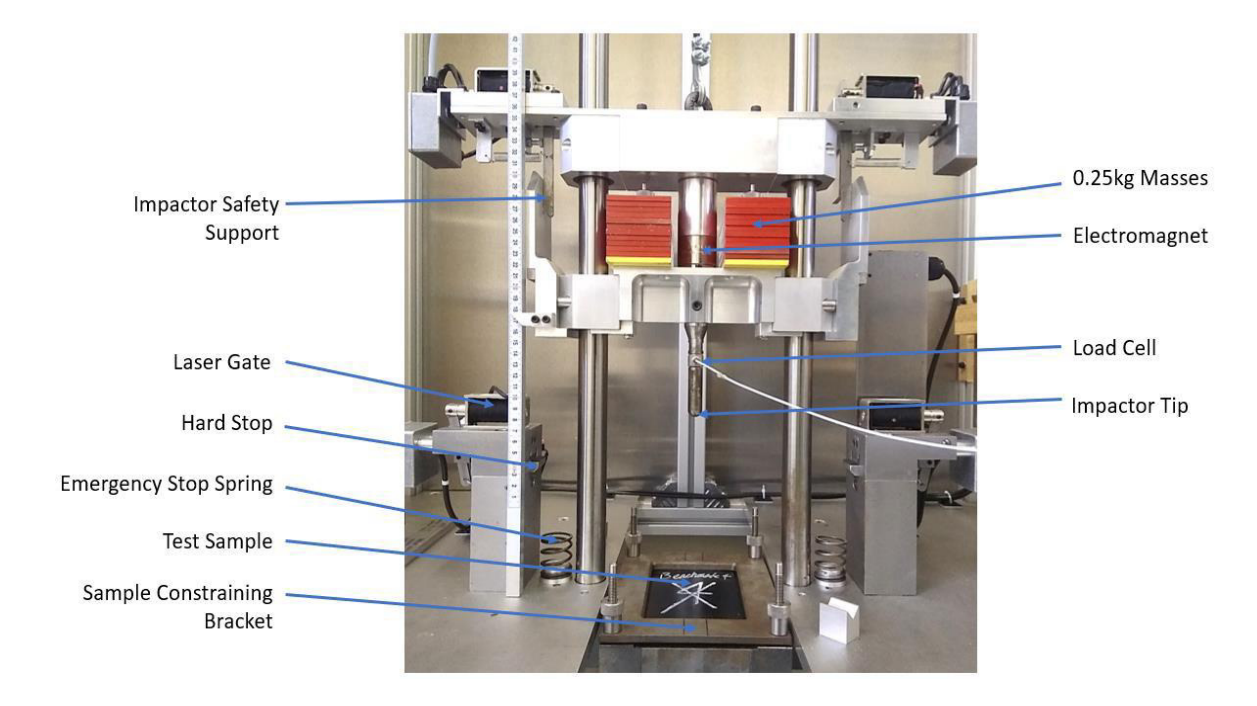


Figure 6-Impact rig used during the impact campaign

For the characterisation of impact behaviour, a selection of impact energies (15J and 25J) was tested for each design, with three samples per impact energy. The energy of the system was varied by the initial height of the dropped mass while holding the impactor mass constant at 8.66kg. An anti-rebound system using two laser gates was used to avoid a second impact on the samples. After impact, in order to correlate the energy absorption profiles with the different failure mechanisms, ultrasonic techniques were used to generate C-scan data with images reporting damage extent and depth information over

the surface plane. The phased array NDT was carried out using an ultrasonic scanner (National Instrument) with an array of 128 transducers to image a 67.3mm wide section of each sample.

In order to characterise the post-impact residual properties of the bioinspired laminates and estimate their residual structural integrity, Flexural After Impact (FAI) tests were carried out. Standard post-impact testing methods including Compression After Impact (CAI) (ISO 18352:2009), commonly used to evaluate these properties, were impossible to apply for FGPA bioinspired configuration used in this work due to significant buckling (not acceptable by the standard) [51] generated during the test related to non-zero extensional-flexural coupling terms in the stiffness matrix of the laminate. Due to the lack of standards for FAI test, three points bending standard (ISO 14125:1998+A1) and previous research works [52, 53] were used as guidelines. Loading and support rollers used in this experimental campaign were 25 mm in diameter, the span between the support rollers was set to 100 mm while the crosshead speed of the loading roller was 4.5mm/minute. The impacted sample is inserted into the machine and the load is applied until a drop of 60% of the maximum recorded load is identified. The post-impact residual energy W_{residual} [J] involved in the process is calculated using equation 23

$$W_{residual} = \int_0^{d_{max}} F \, dx \tag{23}$$

where d_{max} is the displacement reached when the force drops of 60% of the maximum force recorded.

4 Results and Discussion

4.1 Flexural tests

The flexural stress-strain results of benchmark, FGPS and FGPA samples collected using three-point bending testing are shown in Figure 7.

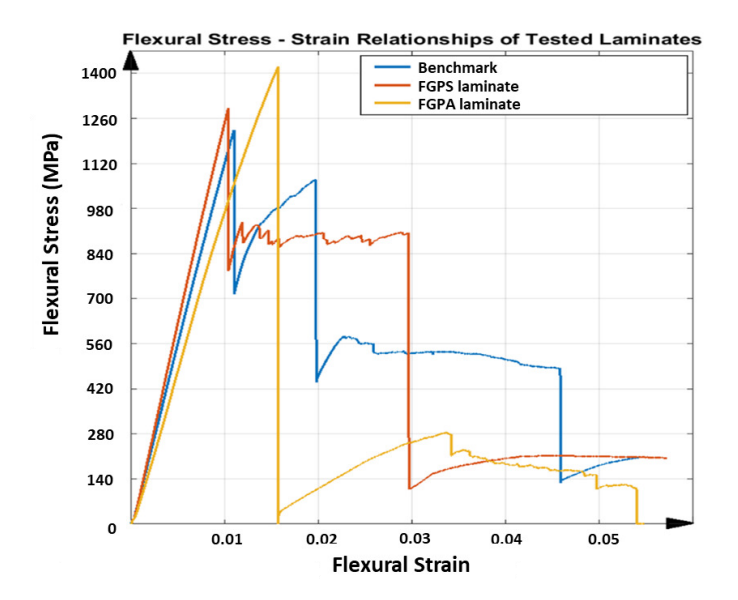
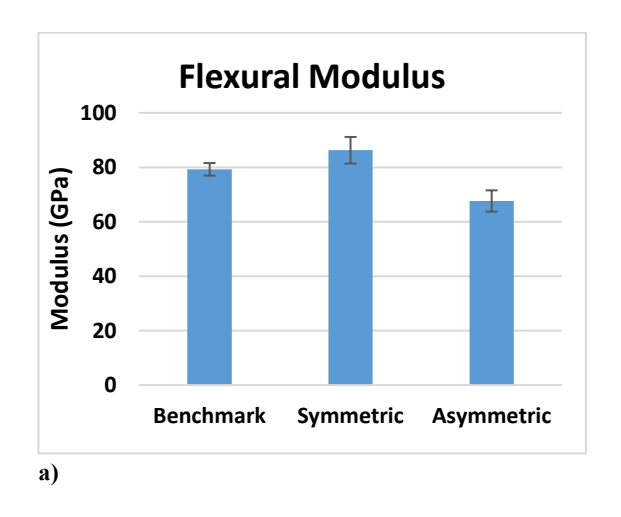
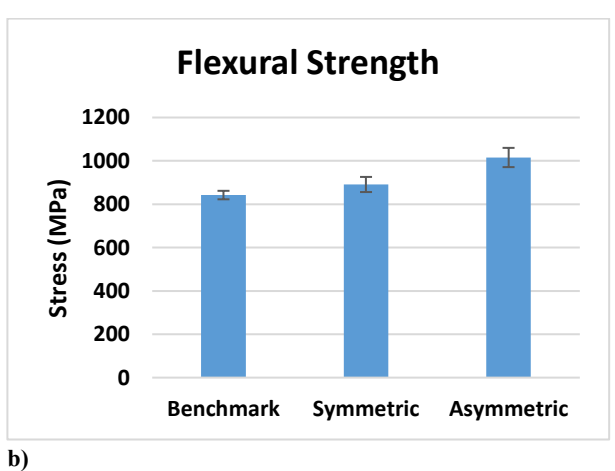
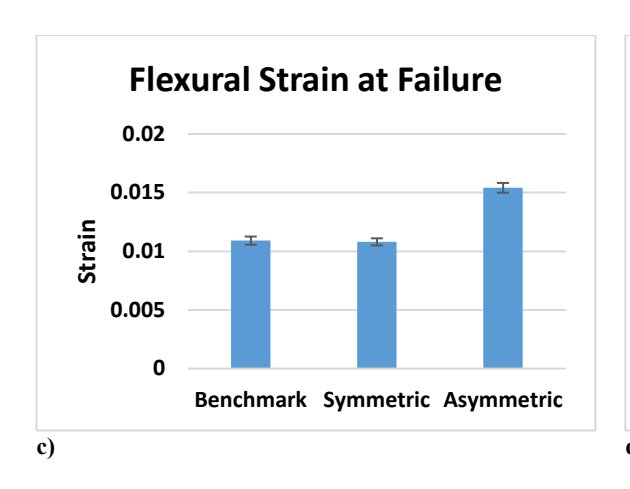


Figure 7- Flexural stress-strain curves for benchmark, symmetric (FGPS) and asymmetric (FGPA) configurations:

Flexural data are reported on Figure 8 where flexural modulus, flexural strength, flexural strain at failure and SEE stored during tests are shown. It is important to notice that the specific elastic energy values are calculated considering the maximum flexural force and the corresponding strain value that represents the flexural strain at failure. Table 2 reports mean and standard deviation of flexural data benchmark, FGPS and FGPA configurations







 $\begin{array}{c} 307 \\ 308 \end{array}$

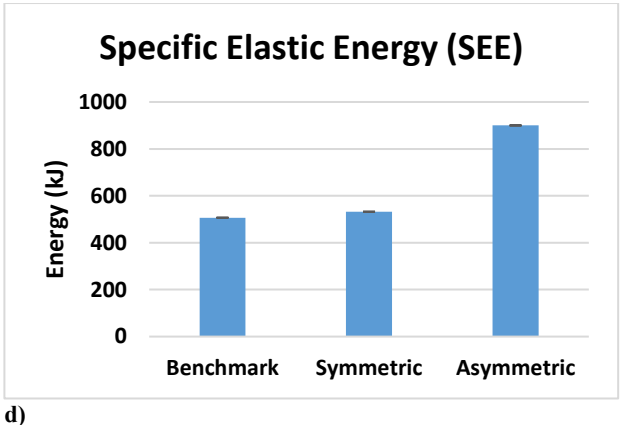


Figure 8- Bar plot results for benchmark, FGPS and FGPA configurations: a) flexural modulus, b) flexural strength and d) flexural strain at maximum force value and e) Specific Elastic Energy (SEE)

Table 2- Mean and standard deviation for flexural data of benchmark, symmetric (FGPS) and asymmetric (FGPA) configurations

Design	Flexural Modulus (GPa)	% variation	Flexura l Strengh t (MPa)	% variation	Flexural strain (Maximum Load)	% variation	SEE (kJ/m	% variation
Benchmark	79.2±2.32	-	842±19. 56	-	0.0109±0.000 35	-	507±2 5	-
FGPS	86.3±4.88	+9%	891±34. 8	+6%	0.0154±0.000 30	-1%	532±2 5	+5%
FGPA	67.6±3.91	-15%	1015±4 4.37	+21%	0.0154±0.000 42	+41%	900±6 3	+78%

As reported in Figure 7, the FGPS configuration shows an initial elastic behaviour similar to the benchmark with a slight variation in flexural modulus (Figure 8.a), flexural strength (Figure 8.b), and elastic energy stored (Figure 8.d) of +9%, +6% and +5% respectively. One can notice that the flexural stress for the FGPS samples remains approximately constant with strain after the initial load drop given by the failure of the top layer and visible damage below the top 0° plies as shown in Figure 9.



Figure 9- Initial Damage Propagation of Benchmark and FGPS laminates

This is divergent from the benchmark behaviour, which experiences a gradual reduction of flexural stress increasing the applied strain. This behaviour can be attributed to the pure delamination case of damage propagation in the benchmark sample, contrasting the more complex evolution of damage downwards in the FGPS laminate. The propagation of this damage through adjacent plies is affected by the higher interlaminar strength provided by the small angle difference between the two plies [17] that eases the crack-jumping from layer to layer [39] without the generation of wide delaminated areas. Once initiated, the crack progressively propagates throughout the laminate's thickness following a tortuous path which dissipates higher amount of energy preventing flexural stress from increasing with strain and generating a plateau region in the stress-strain plot. Due to the reduced stiffness resulting from damage in composites [9], the brittleness of the FGPS is reduced and causes the flexural strain at the secondary load drop to significantly increase.

Analysing the results from FGPA configuration (Figure 7 and Figure 8), it is possible to observe a higher maximum flexural stress (+21%) and strain (+41%) than benchmark one at the first load drop. This behaviour causes a greater amount of energy to be stored in the FGPA laminate (+78% compared to benchmark) before damage, which improves the damage resistance of this configuration by requiring a greater energy to initiate a critical damage. Indeed, FGPA structure initiates damage with a significantly different mechanism than the other tested laminates. This is due to the functionally graded angle used to manufacture the sample as the smaller the pitch angle, the smoother the crack propagation across the different plies, leading to higher damage tolerance and reduced delamination extent [19]. Moreover, due to the small variable angle between the plies, the stiffness of the laminate varies across the thickness as described in Section 2.1. Therefore, in the area where a small angle pitch is used, the lower laminate stiffness allows to store a higher amount of elastic energy in the material

during deformation since virtually no delamination is generated during the failure initiation and propagation due to the activation of crack twisting [18]. On the other hand, in the area where ply angle is greater, a higher value of stiffness is reported that balances the effect of small initial ply angle on the global stiffness of the laminate but, at the same time, induces a higher sensitivity towards the generation of non-critical damage. This is confirmed by observing images in Figure 10 where failure mechanisms are shown, and subcritical stable damage is visible before failure.



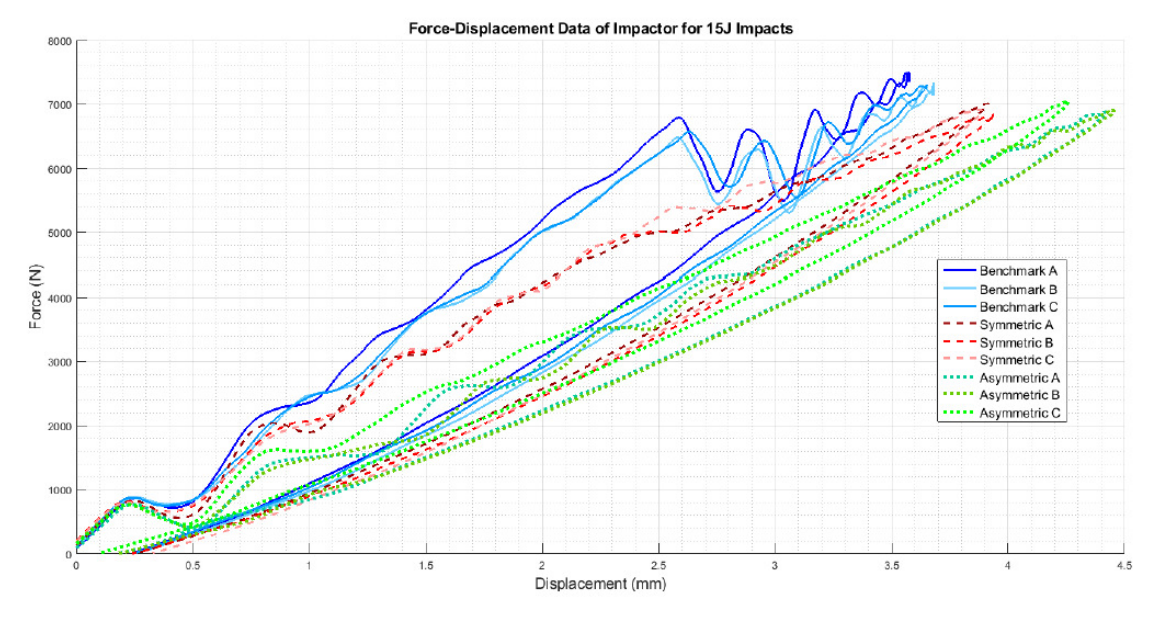
Figure 10- Damage evolution in FGPA laminates: sub-critical damage (top image) and critical damage (bottom images)

The cause of this subcritical damage in the tensile portion is the increasing angle ply that allows the generation of a higher amount of interlaminar damage. However, this subcritical damage is stable and has no tendency in degenerating into an unstable critical one as found, instead, in the benchmark case. In addition, since the failure of the laminate is initiated and dominated by the crack twisting mechanism in the compressive portion, this stable damage generated within the tensile portion has not only a marginal detrimental effect on the mechanical properties of the laminate, but also helps the system to dissipate a higher amount of energy enabling the system to reach an large strain without the critical failure of the interested layers [16]. Thus, even though a reduced stiffness (-15% compared to benchmark) is associated with the presence of these subcritical damage, comparing these configuration with benchmark and FGPS, higher maximum flexural strength in the elastic portion of the curve is identified at a higher strain at failure values.

4.2 Impact tests

Force-displacement data from the 15 and 25J impacts is shown in Figure 11 while impact results including mean and standard deviation of impact force, maximum displacement, damaged area and

absorbed energy are reported in Figure 12. In Table 3, the mean and standard deviation of the impact results for the different configurations are reported.



a)

363

361

362

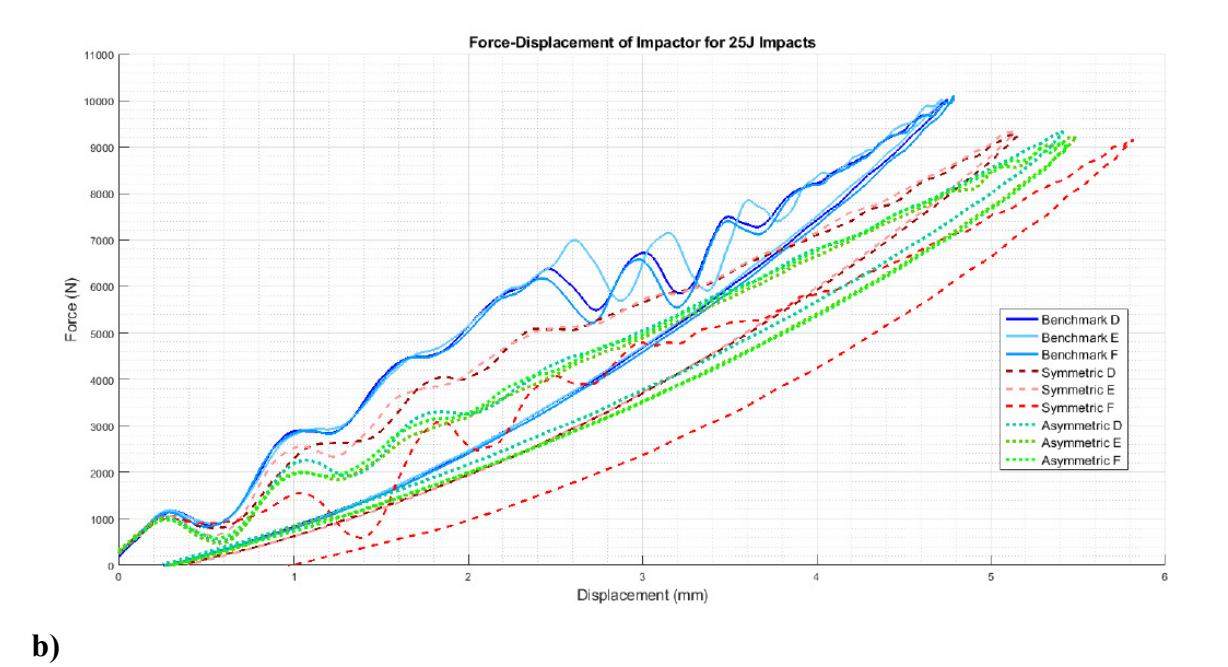
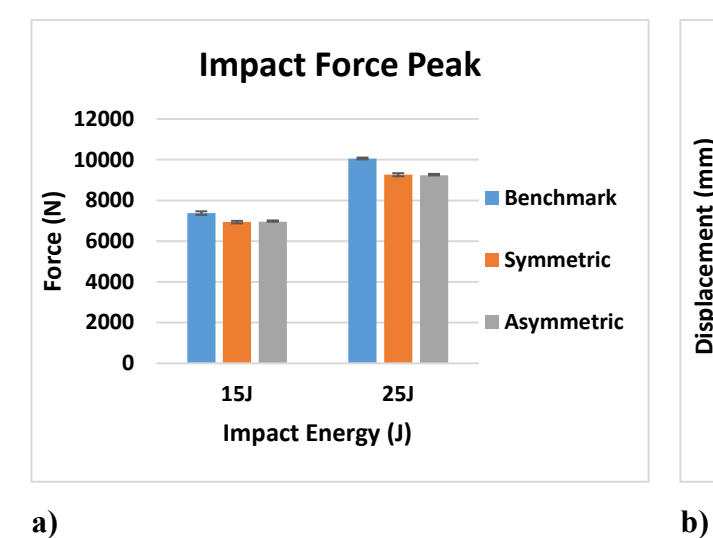
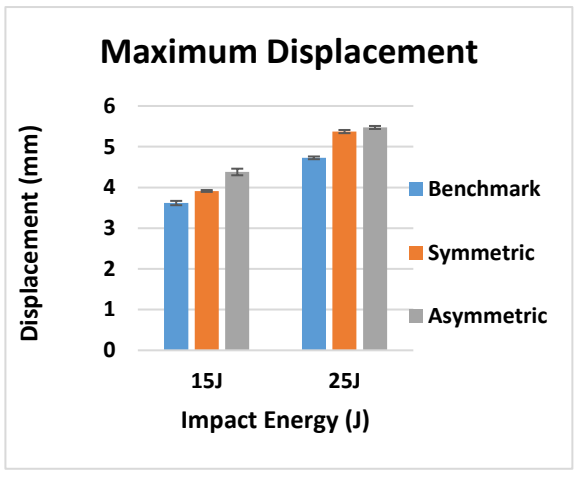


Figure 11-Force-Displacement curves for benchmark, symmetric and asymmetric configurations





Damaged Area

2500
2000
1500
1000
500
0
15J
25J
Impact Energy (J)

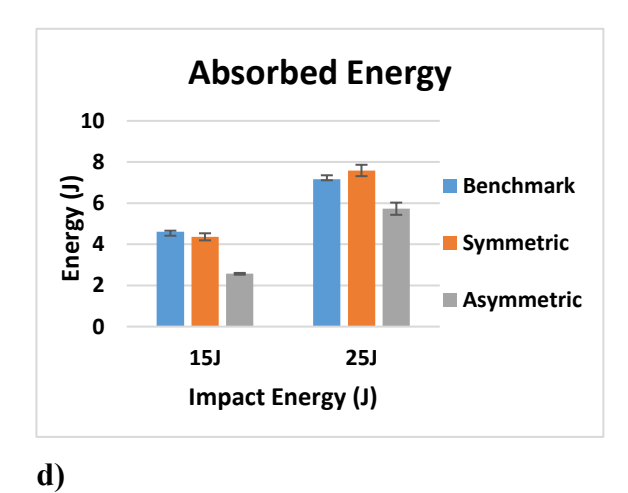


Figure 12- Bar plot with mean and standard deviation of a) impact force peak, b) maximum displacement, c) damaged area and d) absorbed energy for benchmark, symmetric (FGPS) and asymmetric (FGPA) configurations

Table 3- Mean and standard deviation of impact results for Benchmark, Symmetric (FGPS) and Asymmetric (FGPA) configurations

Configuration	Impact Energy (J)	Impact Force Peak (N)	% variation	Maximum displacement (mm)	% variation	Damaged Area (mm²)	% variation	Absrobed Energy (J)	% variation
Benchmark	15	7377.08±88.4	-	3.61±0.052	-	859.97±54.74	-	4.60±0.057	-
Symmetric	15	6934.79±64.54	-6%	3.91±0.022	+8%	1041.12±92.19	+21%	4.36±0.172	-5%
Asymemetric	15	6955.12±62.43	-6%	4.37±0.080	+21%	437.24±106.54	-49%	2.56±0.042	-44%
Benchmark	25	10059.44±44.5 8	-	4.72±0.033	-	1734.86±100.82	-	7.17±0.1857	-
Symmetric	25	9259.95±74.99	-8%	5.37±0.390	+14%	2147.79±54.24	+24%	7.59±0.2763	+6%
Asymemetric	25	9229.94±73.07	-8%	5.47±0.037	+16%	1163.69±79.05	-33%	5.73±0.2970	-20%

Considering the impact curves at 15J in Figure 11.a, it is possible to observe the impact force initially increasing with displacement for all the designs. A slightly reduction in peak impact force for FGPS (-6%) and FGPA (-6%) laminates in comparison with the benchmark is reported showing no

significant load drops, observed instead in the benchmark between ~2-4mm and are typical in laminate damage mechanisms. Moreover, as shown in Table 2 and explained for the flexural tests in Figure 8, higher maximum displacement values are shown for FGPS (+8%) and FGPA (+21%) configurations when compared to the benchmark due to the functionally graded characteristics of in the lamination sequence due to the use of a FGP angle ply that allows a more uniform impact energy distribution along the through the thickness direction of the laminate [54]. Comparing these impact curves with the flexural ones (Figure 7), it is possible to notice a different trend in terms of mechanical stiffness (slope of the curves). This is explained considering the contribute to bending and shear stress on mechanical response of the material for the two different experimental cases. In the flexural case (three points bending condition), standard guidelines are followed by setting the width of the beam to a certain value (15mm) and its span/thickness to 40. This allows to neglect major shear effects during the experimental tests and evaluate mechanical response of pure bending [55]. This translates into a higher stiffness is recorded for FGPS and FGPA configurations in comparison with benchmark since a higher number of plies close to the 0° direction is used in their stacking up sequence. On the contrary, no pure bending condition can be achieved in the impact case (low velocity impact condition) since a plate geometry (150mm x 100mm) is used as described by the standard guidelines leading to sheardominant mechanical response [45]. Consequently, the higher number of plies oriented along 0° has no beneficial effects for the FGPS and FGPA configurations and a lower stiffness is recorded in comparison with benchmark. The energy absorbed by the samples during impact is reported in Figure 12.d, where similar values between FGPS and benchmark laminates are shown. FGPA laminates, instead, reported a reduced energy absorption when compared to benchmark (-44%) that can be correlated to a reduction in damaged area. Thus, in order to investigate the extent and distribution of internal damage of FGPS and FGPA configurations generated as results of the impact loading, a phased array ultrasound technique was used. The time-of-flight C-scans of 15J samples are shown in Figure 13 using a normalised reflection depth scaling (colour map-16 bit) from 0 (white) to 1 (red).

371

372

373

374

375

376

377

378

379

380

381

382

383

384

385

386

387

388

389

390

391

392

393

394

395

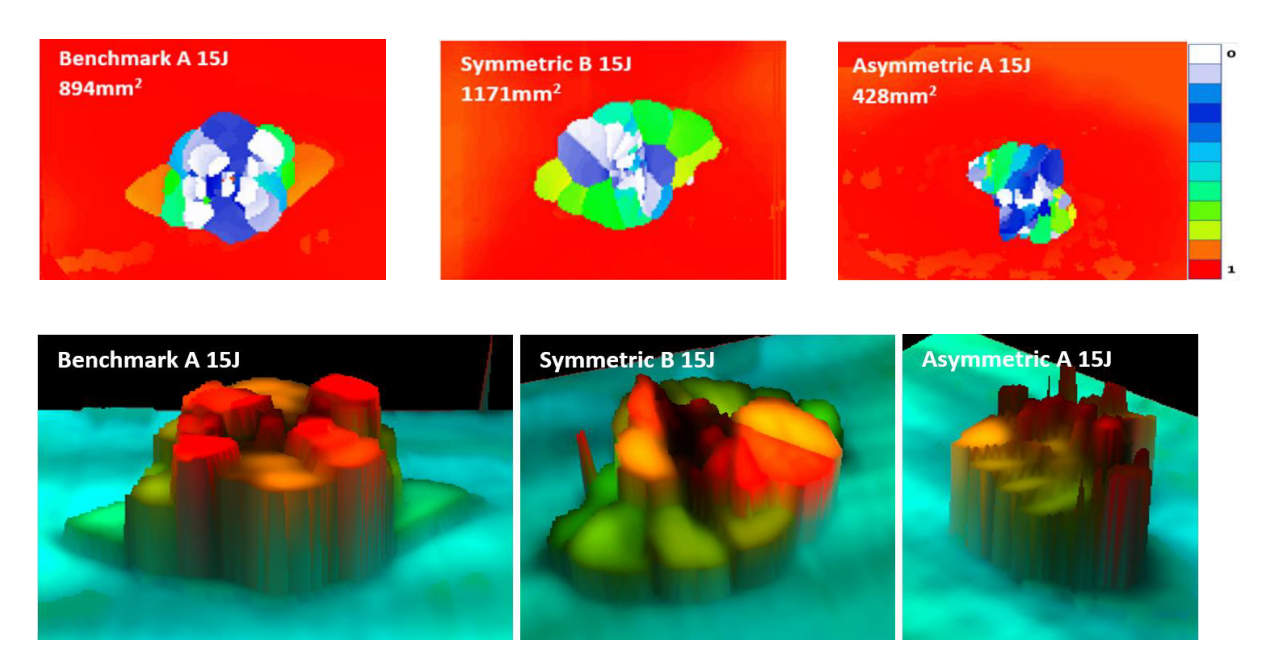


Figure 13- Time-of-Flight C-Scans and 3D images of 15J Impact Samples for Benchmark, symmetric (FGPS) and asymmetric (FGPA) configuration

398

399

400

401

402

403

404

405

406

407

408

409

410

411

412

413

414

415

416

417

As can be seen from images, the benchmark laminate experiences peanut-shaped damage [1], whilst the FGPS and FGPA laminates display alternative damage mechanisms. In the same figure, threedimensional images based on damage depth are shown in order to visualise the shapes of the damage within laminates. As it is possible to see from these images, damage in FGPS and FGPA laminates follows a twisting crack, which acts as a toughening mechanism [17] and reduces the area of delamination. This is due to the ability of helicoidal structures to initiate and propagate the crack along a specific path given by the ply angle. Indeed, as already shown for the flexural data discussion, the crack path in FGP helicoidal laminates is forced to twist following the ply angle that varies along the thickness of the laminate accumulating sub-critical stable damage within laminate's body as also reported by [16] in a similar case of study. This is less detrimental damage topology than delamination that instead is considered an unstable critical one. Damaged area of 15J impact samples is shown in Figure 12.c. FGPS laminates propagate damage over a larger area than the benchmark (+21%) whilst the FGPA laminates have greatly reduced damaged area (-44%). This is due to the variable stiffness across the thickness of the FGPA design also observed during the flexural tests, which enables the laminate to store a higher amount of elastic energy during the dynamic event and consequently to reduce the amount that is dissipated via the creation of new surfaces [56]. Figure 11.b shows reduced peak force for the helicoidal laminates at 25J impacts when compared to the benchmark ones. In particular, the FGPS configuration shows a variation in force peak and maximum displacement of -8% and +14% respectively compared to benchmark, while FGPA illustrates a force peak reduction of -8% and a maximum displacement variation of +16%. Slight load drops are visible in both helicoidal configurations near peak force at this energy, which indicates reduced stiffness from structural damage. Figure 12.d shows the absorbed energy of FGPS laminates which slightly exceeds the benchmark at 25J impact energy (+6%), whilst the FGPA laminate is characterised by reduced energy absorption. The crack twisting mechanism contributing to energy absorption are visible in ultrasonic C-scans and 3D damage images in Figure 14 where it is possible to observe how the crack is able to rotate during propagation accordingly to the used ply angle.

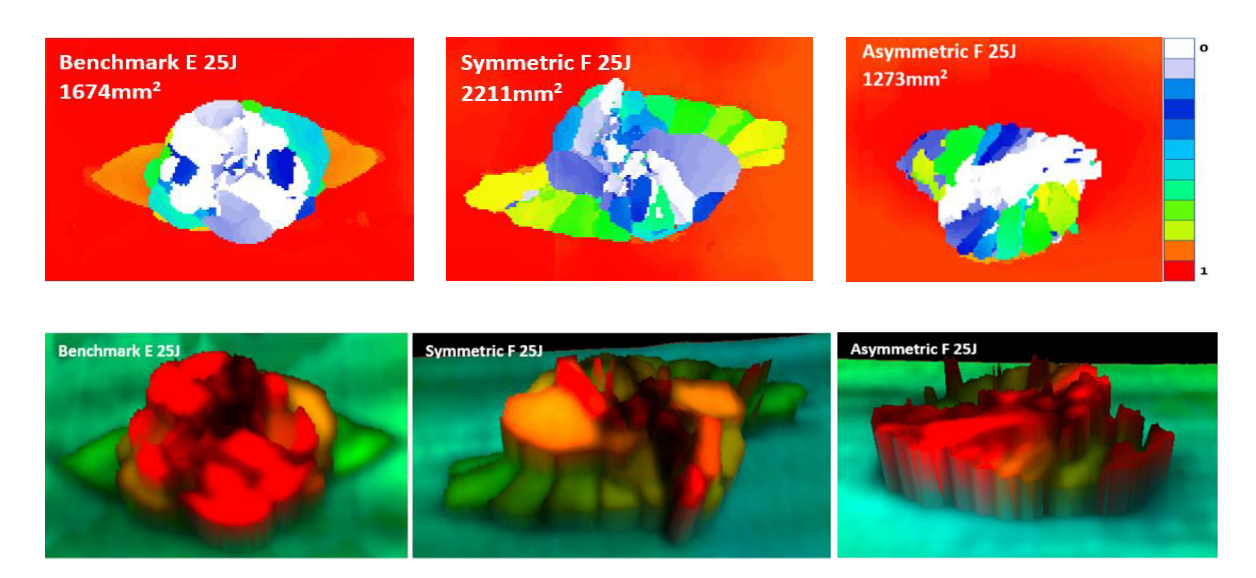


Figure 14- Time-of-Flight C-Scans and 3D images of 25J Impact Samples for Benchmark, symmetric (FGPS) and asymmetric (FGPA) configuration

As it is possible to see from the images, the different configurations show similar damage shapes between 15J (Figure 13) and 25J impacts with larger damage propagation for 25J case. 3D images also show twisting cracks in both helicoidal laminate designs with the propagation of crack front oriented accordingly to the local ply angle, indicating that these designs successfully exploit this toughening mechanism minimising the generation of delaminated areas. Analysing the damaged area reported in Figure 12.c, it is possible to notice a similar trend in the extent of damaged area between 15J and 25J cases with increase for FGPS laminates and reduction for FGPA one when compared to the benchmark. In order to confirm the ability of these bioinspired structures in improving the damage tolerance when introduced into a laminated composite, Flexural After Impact (FAI) tests were carried out on the impacted samples and the output results are reported in **Error! Reference source not found.**

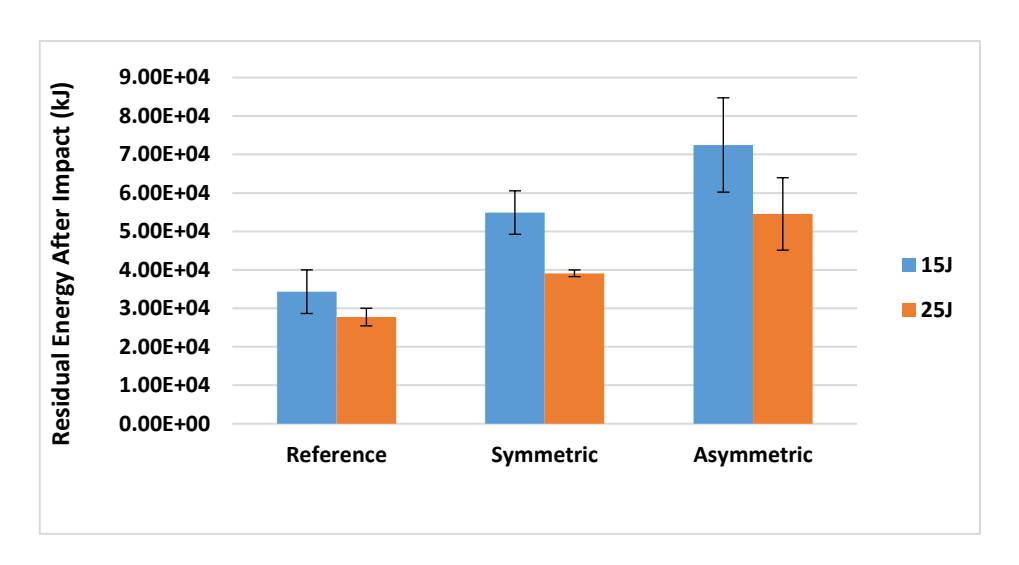


Figure 15- Results of FAI tests

Table 4- Data for FAI tests reporting the mean of residual energy (kJ) and relative variation from benchmark for each configuration (FGPS and FGPA).

Residual Energy (kJ)	15J	% Variation	25J	% Variation	Standard Deviation	15J	25J
Benchmark	3.43e+04	0%	2.77e+04	0%	Benchmark	5.66e+03	2.30e+03
FGPS	5.49e+04	60%	3.91e+04	41%	FGPS	5.65e+03	8.68e+02
FGPA	7.25e+04	111%	5.45e+04	97%	FGPA	1.23e+04	9.41e+03

Analysing the data in this figure, it is clear that all the configurations impacted at 15J show a higher post-impact residual energy than the ones impacted at 25J since a greater damaged area is generated within the laminate. A significant difference is identified between the bioinspired and traditional configurations reporting, at 15J, an increase of post-impact residual energy of +60% and +111% for FGPS and FGPA when compared with the benchmark configuration. Similarly, at 25J, the post-impact energy residual is +41% (FGPS) and +97% (FGPA) higher than the one of the benchmark confirming the ability of these bioinspired structures of promoting the propagation of twisted cracks within the laminate that generate subcritical damage and minimise the number of delaminated areas within the part. Thus, since the structure integrity is less compromised, the two bioinspired structures can store a higher amount of energy than traditional ones when transversally loaded after an impact event. Comparing the results obtained between the bioinspired configurations, instead, the FGPA configuration shows a higher residual energy than the FGPS one since a smaller damaged area is identified within the laminate's body. This can be attributed to the efficiency of this structure in maximising the benefits of twisting-crack mechanisms given by the smoother variable stiffness across

the laminate's thickness and the reduced extent of delaminated areas generated during the impact event.

5 Conclusions

452

- 453 The ability of a helicoidal laminates featuring a novel Functionally Graded (FGP) layup sequence in 454 improving the impact performance of CFRP laminates has been explored via static three-point bending 455 and impact testing. Both symmetrical (initial/final angle: 5/40°) and asymmetric (initial/final angle: 456 1.2/20°) helicoidal designs (FGPS and FGPA respectively) demonstrated enhanced twisting-crack 457 damage mechanisms, which mimics in detail the behaviour of biological structures including the dactyl 458 club of the Mantis Shrimp. The successful replication and activation of this unique failure mechanisms 459 was confirmed by photograph evidence revealing extensive matrix twisted cracking in bending 460 samples. The Functionally Graded Symmetric (FGPS) helicoidal laminate shows slight improvement in flexural 461
- 462 strength (+6%) and modulus (+9%) pointed out from three-points bending tests. On the other hand, no 463 significant load drops and reduced peak impact force (6-8%) are identified from impact results for both 464 the impact energies considered during impact testing (15J and 25J). However, the reduction in 465 damaged area (~21-24%) and increase in post-impact residual energy (41-60%) in comparison with 466 the traditional laminates used as benchmarks indicates this design is successful in fully exploiting the 467 helicoidal architecture in improving toughness. This is due to crack twisting failure mechanism that 468 dissipates large quantities of impact energy in creating stable matrix cracks instead of unstable 469 delaminated areas as shown in post-impact phased array testing.
- 470 The Functionally Graded Asymmetric (FGPA) helicoidal laminate reports instead greatly reduced 471 impact damaged area (-33-49%), the absorbed energy (-20-44%), and a significant increase in post-472 impact residual energy (91-111%). In addition, this structure shows in flexural loading conditions 473 greater mechanical strength (21%) and elastic strain (+41%). The reason of this improved flexural and 474 impact behaviour can be found in the coupling effect between crack twisting and variable stiffness 475 along the thickness of the laminate that allows for storing a higher amount of impact energy elastically 476 and dissipate efficiently the excess via sub-critical twisted cracks that reduces the delaminated areas 477 increasing the residual mechanical properties of the part.
- Based on these results, FGPA configuration can express its full potential in applications where a superior impact resistance and damage tolerance are mandatory for the safety and reliability of the global structure

FGPS configuration, instead, can be successfully utilised as alternative to the FGPA configuration in order to improve impact response of composite material in all those applications where a geometrical stability and damage tolerance are required.

484

485

Appendix A - Thermal warpage

In order to analyse the thermal behaviour of helicoidal configurations and, understand the design limitation given by potential residual thermal stresses, analytical methods were used. Classical laminate theory [57] can be applied in a plane stress state, which first requires calculation of the local coordinate lamina stiffness matrix given by Equation (7).

$$[C] = \begin{bmatrix} C_{11} & C_{12} & 0 \\ C_{21} & C_{22} & 0 \\ 0 & 0 & C_{66} \end{bmatrix}$$
 (7)

490 with:

$$C_{11} = \frac{E_{11}}{1 - v_{12}v_{21}} \tag{8}$$

$$C_{22} = \frac{E_{22}}{1 - v_{12}v_{21}} \tag{9}$$

$$C_{12} = C_{21} = \frac{v_{12}E_{22}}{1 - v_{12}v_{21}} = \frac{v_{21}E_{11}}{1 - v_{12}v_{21}}$$
(10)

$$C_{66} = G_{12} \tag{11}$$

Where [C] is the local coordinate lamina stiffness matrix, E_{11} is the longitudinal Young's Modulus of the lamina (~135GPa), E_{22} is the transverse Young's Modulus (~8.5GPa), v_{12} is the major Poisson's Ratio (~0.33), v_{21} is the minor Poisson's Ratio (~0.021) and G_{12} is the Shear Modulus (~5GPa). Using the transformation matrix in Equation (7), Equation (12) is used to obtain the local stiffness matrix of each lamina to the global coordinate system.

$$[T] = \begin{bmatrix} \cos^2 \theta & \sin^2 \theta & \frac{1}{2} \sin 2\theta \\ \sin^2 \theta & \cos^2 \theta & -\frac{1}{2} \sin 2\theta \\ -\sin 2\theta & \sin 2\theta & \cos 2\theta \end{bmatrix}$$
(12)

$$[Q] = [T]^t [C] [T] \tag{13}$$

where [T] is the transformation matrix, θ is the lamina rotation angle and [Q] is the lamina stiffness matrix in global coordinates. Calculating the [Q] matrices for all laminae enables computation of the behaviour-defining [A], [B], and [D] matrices from Equations (14)-(16).

$$[A] = \sum_{k=1}^{N} [Q_k] t_k \tag{14}$$

$$[B] = \sum_{k=1}^{N} [Q_k] t_k \overline{z_k}$$
 (15)

$$[D] = \sum_{k=1}^{N} [Q_k] \left(t_k \, \overline{z_k}^2 + \frac{t_k^3}{12} \right) \tag{16}$$

Where [A] is the laminate membrane stiffness matrix, [B] is the laminate coupling matrix, [D] is the laminate bending stiffness matrix, t is the thickness of a single ply, \bar{z} is the mean average height of each ply from the laminate midplane.

502

503

504

Table 5 data were calculated for each configuration using Equations 14,15 and 16 and considering the lamination sequences reported in Table 1.

Table 5-Composite Laminate Matrices

	Benchmark
[A] Matrix:	\[\begin{pmatrix} 341.32 & 82.75 & 0 \ 82.75 & 268.26 & 0 \ 0 & 0 & 93.98 \end{pmatrix} \text{kN/mm} \]
[B] Matrix:	$\begin{bmatrix} 0 & 0 & 0 \\ 0 & 0 & 0 \\ 0 & 0 & 0 \end{bmatrix} kN$
[D] Matrix:	[1075.86 146.39 24.04] 146.39 352.70 24.04 24.04 24.04 171.34] kNmm
F	unctionally Graded Helicoidal Symmetric
[A] Matrix:	[409.49 73.71 39.97] 73.71 218.16 16.28 kN/mm 39.97 16.28 84.94]

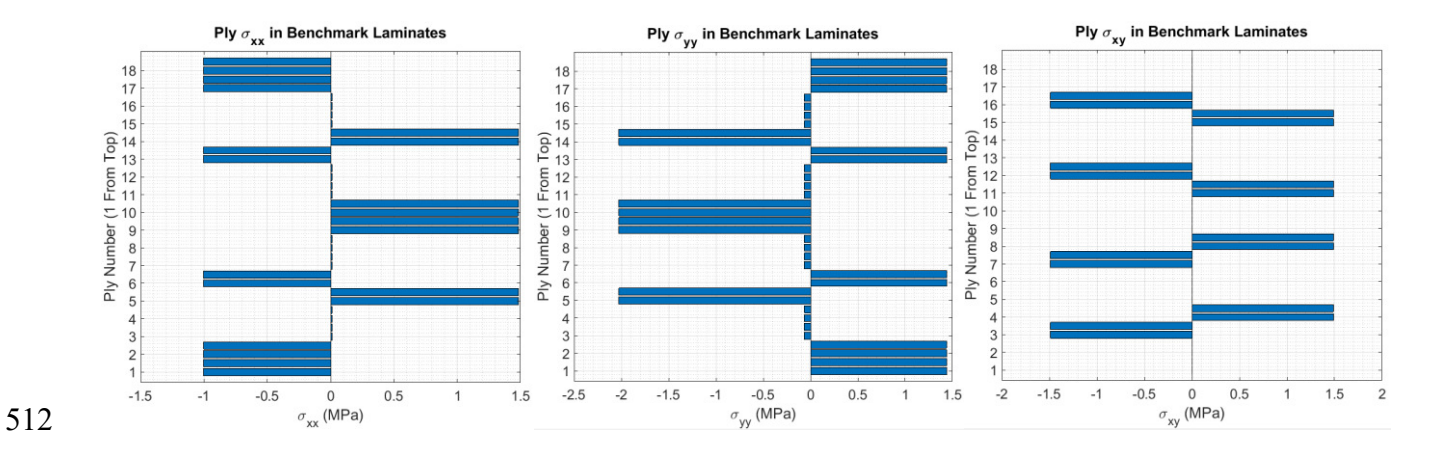
[B] Matrix:	$\begin{bmatrix} 0 & 0 & 0 \\ 0 & 0 & 0 \\ 0 & 0 & 0 \end{bmatrix} kN$
[D] Matrix:	[1224.64 118.85 165.64] 118.85 259.01 68.57 165.64 68.57 143.79] kNmm
Fi	unctionally Graded Helicoidal Asymmetric
[A] Matrix:	[399.12 75.98 38.46] 75.98 223.99 17.16 38.46 17.16 87.21] kN/mm
[B] Matrix:	[207.27 -28.52 93.77 -28.52 -150.22 44.22 93.77 44.22 -28.52
[D] Matrix:	[1213.94 112.65 -47.60] 112.65 282.11 -65.66 -47.60 -65.66 137.59]

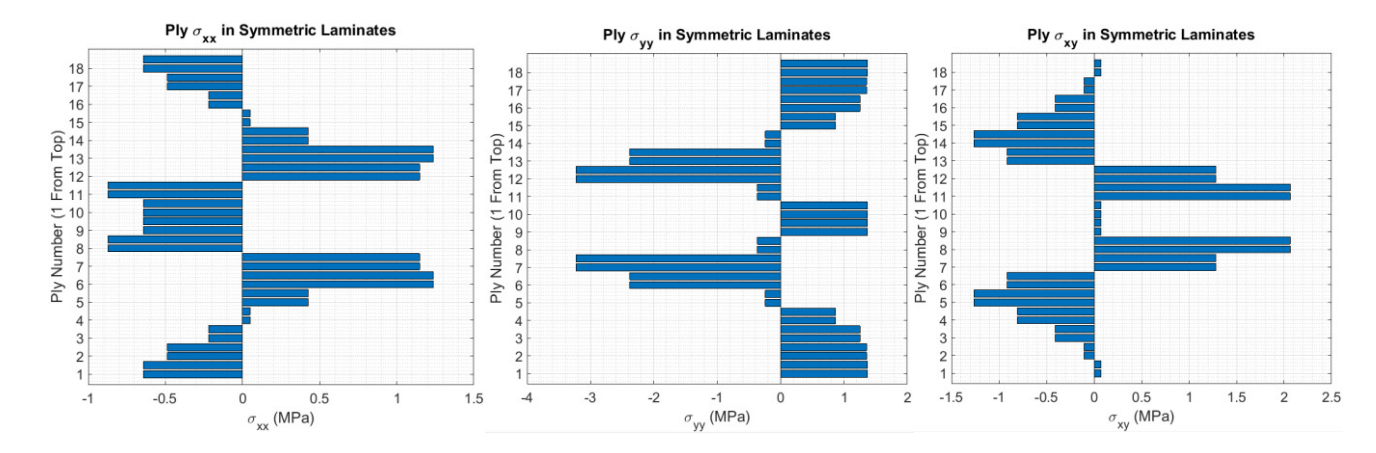
The thermal stresses induced from cooling after the elevated temperature autoclave cycle are calculated per Equation (17).

$$\{\sigma\}^k = [C]^k \left(\{\varepsilon\}^k - \{\alpha_T\}^k \Delta T\right) \tag{17}$$

Where $\sigma^{(k)}$ is local stress vector of k^{th} ply, [C] is local stiffness matrix of k^{th} ply, $\epsilon^{(k)}$ is local strain vector of k^{th} ply, $\alpha_T^{(k)}$ is thermal expansion coefficient vector of k^{th} ply, ΔT is change in temperature after cure.

511 Applying Equation (17) resulted in residual thermal stresses described in Figure 16.





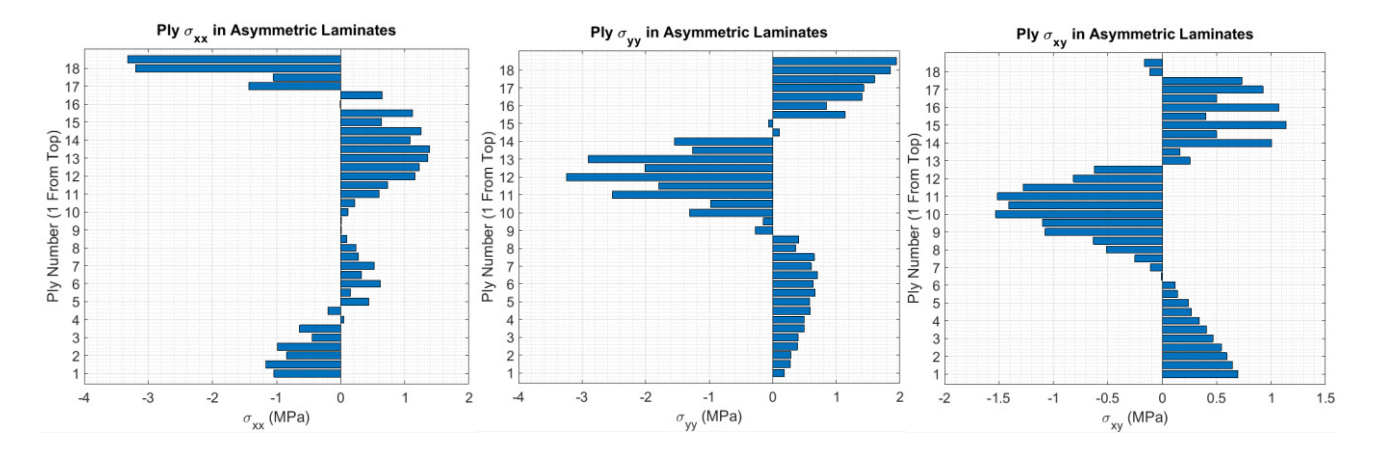


Figure 16- Laminate Residual Thermal Stresses

- As can be seen from this figure, the non-zero [B] matrix in FGPA laminates causes in-plane to
- out-of-plane coupling of forces and deformations leading to thermal-induced warpage and
- 520 twist. Consequently, the thermal residual stress on FGPA samples requires a custom cure cycle
- 521 to be minimised with low curing temperature and cool rate.
- 522 FGPS configuration, instead, was designed using a greater variable ply angle and a symmetrical
- 523 layup obtaining a zero [B] matrix that generates no thermal residual stress on the laminate
- geometry during the cure (Figure 16).

526

References

- 527 [1] Abrate S. Impact on laminated composite materials. Appl Mech
- 528 Rev. 1991;44:155-90.
- 529 [2] Russell AJ, Street KN. The effect of matrix toughness on
- delamination: static and fatigue fracture under mode II shear loading of
- 531 graphite fiber composites. Toughened composites: ASTM
- 532 International; 1987.
- 533 [3] Ning J, Zhang J, Pan Y, Guo J. Fabrication and mechanical
- properties of SiO2 matrix composites reinforced by carbon nanotube.
- Materials Science and Engineering: A. 2003;357:392-6.
- 536 [4] Cho J, Chen J, Daniel I. Mechanical enhancement of carbon
- 537 fiber/epoxy composites by graphite nanoplatelet reinforcement. Scripta
- 538 materialia. 2007;56:685-8.
- [5] Rizzo F, Pinto F, Meo M. Development of multifunctional hybrid
- 540 metal/carbon composite structures. Composite Structures.
- 541 2019;222:110907.
- 542 [6] Rizzo F, Pinto F, Meo M. Investigation of Silica-Based Shear
- 543 Thickening Fluid in Enhancing Composite Impact Resistance. Applied
- Composite Materials. 2020:1-21.
- 545 [7] Rizzo F, Cuomo S, Pinto F, Pucillo G, Meo M. Thermoplastic
- 546 polyurethane composites for railway applications: Experimental and
- numerical study of hybrid laminates with improved impact resistance.
- 548 Journal of Thermoplastic Composite Materials.
- 549 2019:0892705719856049.

- [8] Heinemann F, Launspach M, Gries K, Fritz M. Gastropod nacre:
- structure, properties and growth—biological, chemical and physical
- basics. Biophysical chemistry. 2011;153:126-53.
- 553 [9] Zaheri A, Fenner JS, Russell BP, Restrepo D, Daly M, Wang D, et
- al. Revealing the mechanics of helicoidal composites through additive
- 555 manufacturing and beetle developmental stage analysis. Advanced
- 556 Functional Materials. 2018;28:1803073.
- 557 [10] Suksangpanya N, Yaraghi NA, Kisailus D, Zavattieri P. Twisting
- cracks in Bouligand structures. Journal of the mechanical behavior of
- biomedical materials. 2017;76:38-57.
- 560 [11] Sun J, Bhushan B. Hierarchical structure and mechanical
- properties of nacre: a review. Rsc Advances. 2012;2:7617-32.
- 562 [12] Rizzo F, Pinto F, Meo M. 3D bio-inspired hierarchical
- discontinuous CFRP with enhanced ductility. Composite Structures.
- 564 2019;226:111202.
- [13] Zimmermann EA, Gludovatz B, Schaible E, Dave NK, Yang W,
- Meyers MA, et al. Mechanical adaptability of the Bouligand-type
- 567 structure in natural dermal armour. Nature communications.
- 568 2013;4:2634.
- 569 [14] Cheng L, Wang L, Karlsson AM. Mechanics-based analysis of
- selected features of the exoskeletal microstructure of Popillia japonica.
- Journal of Materials Research. 2009;24:3253-67.
- 572 [15] Vincent JF. Arthropod cuticle: a natural composite shell system.
- 573 Composites Part A: Applied Science and Manufacturing.
- 574 2002;33:1311-5.
- 575 [16] Mencattelli L, Pinho ST. Realising bio-inspired impact damage-
- 576 tolerant thin-ply CFRP Bouligand structures via promoting diffused
- 577 sub-critical helicoidal damage. Composites Science and Technology.
- 578 2019:107684.
- [17] Suksangpanya N, Yaraghi NA, Pipes RB, Kisailus D, Zavattieri P.
- 580 Crack twisting and toughening strategies in Bouligand architectures.
- International Journal of Solids and Structures. 2018;150:83-106.
- 582 [18] Shang J, Ngern NH, Tan VB. Crustacean-inspired helicoidal
- laminates. Composites Science and Technology. 2016;128:222-32.

- [19] Ginzburg D, Pinto F, Iervolino O, Meo M. Damage tolerance of
- 585 bio-inspired helicoidal composites under low velocity impact.
- 586 Composite Structures. 2017;161:187-203.
- 587 [20] Grunenfelder L, Suksangpanya N, Salinas C, Milliron G, Yaraghi
- N, Herrera S, et al. Bio-inspired impact-resistant composites. Acta
- 589 biomaterialia. 2014;10:3997-4008.
- 590 [21] Mahamood RM, Akinlabi ET, Shukla M, Pityana S. Functionally
- 591 graded material: an overview. 2012.
- 592 [22] Pagano N, Hatfield HJ. Elastic behavior of multilayered
- bidirectional composites. AIAA journal. 1972;10:931-3.
- 594 [23] Erdogan F. Fracture mechanics of functionally graded materials.
- 595 Composites Engineering. 1995;5:753-70.
- 596 [24] Gu P, Asaro R. Cracks in functionally graded materials.
- 597 International Journal of Solids and Structures. 1997;34:1-17.
- 598 [25] Bao G, Cai H. Delamination cracking in functionally graded
- coating/metal substrate systems. Acta Materialia. 1997;45:1055-66.
- [26] Liu Z, Meyers MA, Zhang Z, Ritchie RO. Functional gradients
- and heterogeneities in biological materials: Design principles,
- functions, and bioinspired applications. Progress in Materials Science.
- 603 2017;88:467-98.
- 604 [27] Sola A, Bellucci D, Cannillo V. Functionally graded materials for
- orthopedic applications-an update on design and manufacturing.
- Biotechnology advances. 2016;34:504-31.
- [28] Sun C-Y, Chen P-Y. Structural design and mechanical behavior of
- 608 alligator (Alligator mississippiensis) osteoderms. Acta biomaterialia.
- 609 2013;9:9049-64.
- [29] Degtyar E, Harrington MJ, Politi Y, Fratzl P. The Mechanical Role
- of Metal Ions in Biogenic Protein Based Materials. Angewandte
- Chemie International Edition. 2014;53:12026-44.
- [30] Peisker H, Michels J, Gorb SN. Evidence for a material gradient
- in the adhesive tarsal setae of the ladybird beetle Coccinella
- septempunctata. Nature communications. 2013;4:1-7.

- [31] Chen IH, Yang W, Meyers MA. Alligator osteoderms: mechanical
- 617 behavior and hierarchical structure. Materials Science and
- 618 Engineering: C. 2014;35:441-8.
- [32] Raabe D, Sachs C, Romano P. The crustacean exoskeleton as an
- 620 example of a structurally and mechanically graded biological
- nanocomposite material. Acta Materialia. 2005;53:4281-92.
- [33] Chen P-Y, Lin AY-M, McKittrick J, Meyers MA. Structure and
- 623 mechanical properties of crab exoskeletons. Acta biomaterialia.
- 624 2008;4:587-96.
- 625 [34] Liu Z, Jiao D, Weng Z, Zhang Z. Structure and mechanical
- 626 behaviors of protective armored pangolin scales and effects of
- 627 hydration and orientation. Journal of the mechanical behavior of
- 628 biomedical materials. 2016;56:165-74.
- [35] Wang B, Yang W, Sherman VR, Meyers MA. Pangolin armor:
- overlapping, structure, and mechanical properties of the keratinous
- scales. Acta biomaterialia. 2016;41:60-74.
- [36] Friedrich K. Application of fracture mechanics to composite
- materials: Elsevier, 2012.
- [37] Liu J, Lee H, Tan V. Failure mechanisms in bioinspired helicoidal
- laminates. Composites Science and Technology. 2018;157:99-106.
- [38] Andersons J, König M. Dependence of fracture toughness of
- 637 composite laminates on interface ply orientations and delamination
- growth direction. Composites Science and Technology. 2004;64:2139-
- 639 52.
- [39] Tao J, Sun C. Influence of ply orientation on delamination in
- composite laminates. Journal of composite materials. 1998;32:1933-
- 642 47.
- [40] Kim BW, Mayer AH. Influence of fiber direction and mixed-mode
- ratio on delamination fracture toughness of carbon/epoxy laminates.
- 645 Composites Science and Technology. 2003;63:695-713.
- 646 [41] Riccio A, Linde P, Raimondo A, Buompane A, Sellitto A. On the
- use of selective stitching in stiffened composite panels to prevent skin-
- stringer debonding. Composites Part B: Engineering. 2017;124:64-75.

- [42] Sellitto A, Saputo S, Di Caprio F, Riccio A, Russo A, Acanfora V.
- Numerical-experimental correlation of impact-induced damages in
- cfrp laminates. Applied Sciences. 2019;9:2372.
- 652 [43] Riccio A, Russo A, Sellitto A, Toscano C, Alfano D, Zarrelli M.
- 653 Experimental and Numerical Assessment of Fibre Bridging
- Toughening Effects on the Compressive Behaviour of Delaminated
- 655 Composite Plates. Polymers. 2020;12:554.
- 656 [44] Liu J, Lee H, Tan V. Effects of inter-ply angles on the failure
- 657 mechanisms in bioinspired helicoidal laminates. Composites Science
- and Technology. 2018;165:282-9.
- 659 [45] Abrate S. Impact Dynamics. Impact Engineering of Composite
- 660 Structures: Springer; 2011. p. 71-96.
- [46] Vasiliev VV, Morozov EV. Chapter 3 Mechanics of Laminates.
- 662 In: Vasiliev VV, Morozov EV, editors. Advanced Mechanics of
- 663 Composite Materials and Structures (Fourth Edition): Elsevier; 2018.
- 664 p. 191-242.
- 665 [47] Weaver JC, Milliron GW, Miserez A, Evans-Lutterodt K, Herrera
- 666 S, Gallana I, et al. The stomatopod dactyl club: a formidable damage-
- tolerant biological hammer. Science. 2012;336:1275-80.
- 668 [48] Cheng L, Wang L, Karlsson AM. Image analyses of two
- 669 crustacean exoskeletons and implications of the exoskeletal
- 670 microstructure on the mechanical behavior. Journal of Materials
- 671 Research. 2008;23:2854-72.
- [49] Radford D, Rennick T. Separating sources of manufacturing
- distortion in laminated composites. Journal of Reinforced Plastics and
- 674 Composites. 2000;19:621-41.
- 675 [50] Swanson SR. Limits of quasi-static solutions in impact of
- composite structures. Composites Engineering. 1992;2:261-7.
- [51] Sun C, Chin H. Analysis of asymmetric composite laminates.
- 678 AIAA journal. 1988;26:714-8.
- 679 [52] Santiuste C, Sánchez-Sáez S, Barbero E. Residual flexural
- strength after low-velocity impact in glass/polyester composite beams.
- 681 Composite Structures. 2010;92:25-30.

- [53] Zhang Za, Richardson M. Low velocity impact induced damage
- evaluation and its effect on the residual flexural properties of pultruded
- 684 GRP composites. Composite Structures. 2007;81:195-201.
- 685 [54] Apichattrabrut T, Ravi-Chandar K. Helicoidal Composites.
- Mechanics of Advanced Materials and Structures. 2006;13:61-76.
- [55] Iyer H. The effects of shear deformation in rectangular and wide
- flange sections: Virginia Tech, 2005.
- [56] Anderson TL. Fracture mechanics: fundamentals and applications:
- 690 CRC press, 2017.

[57] Jones RM. Mechanics of composite materials: CRC press, 2014.